**Supporting Information for**

**Efficient photoelectrocatalytic  $CO_2$ reduction to $CH_3OH$ via porous g-$C_3N_4$**

**nanosheets modified with cobalt phthalocyanine in ionic liquids**

Pengyan Li, Yuhang Lin, Zhenhong Qi, Dongpeng Yan[*]

Beijing Key Laboratory of Energy Conversion and Storage Materials, College of Chemistry, and Key Laboratory of Radiopharmaceuticals, Ministry of Education, Beijing Normal University, Beijing 100875, P. R. China.

Corresponding Author

[*]E-mail: yandp@bnu.edu.cn

## 1. Materials and characterizations

### 1.1 Chemicals

Urea (AR, 99%), hydrochloric acid (36−38wt%), cobalt phthalocyanine (AR, 97%), dimethyl sulfoxide, $D_2O$, $C_8H_{15}N_2Br$, ([BMIm]Br, 98%), $C_9H_{17}BrN_2$, ([BMMIm]Br, 98%), $C_{11}H_{21}BrN_2$, ([HMMIm]Br, 98%), $C_9H_{17}BF_4N_2$, ([BMMIm]BF$_4$, 98%), $C_2H_6O$ (AR, 99%), $C_3H_8O$ (AR, 99%), Nafion dispersant (5wt%). All chemicals and solvents were purchased from commercial companies, and deionized water was used in all experiments.

### 1.2 Characterizations

Power X-ray diffraction (PXRD) analysis of the catalysts was performed with a scan rate of 5° min$^{-1}$. The morphology of the CoPc/CN was observed by high resolution transmission electron microscopy (HRTEM) with a Talos F200 FEI TEM microscope operated at 200 keV. The distributions of C, N, and Co in the nanocomposite were determined using energy dispersive spectroscopy (EDS). The optical properties of the photocatalysts were measured through UV–Vis diffuse reflection spectroscopy (UV–Vis DRS). Photoluminescence (PL) spectroscopy was used to analyze the carrier separation efficiency and exciton binding energy in the temperature range from 77 K to 350 K on FS980, and the excitation wavelength is set at 370 nm according to the excitation spectrum. The content of Co was quantitated by inductively coupled plasma (ICP). The environments and interaction between CoPc and CN were tested by X-ray photoelectron spectroscopy (XPS). We carried out BET-related tests and discussions on porous materials, including specific surface area and pore size distribution. The in–situ FT–IR spectra were loaded by using an in–situ cell. The in–situ EPR (electron paramagnetic resonance) signals were recorded in a quartz tube. Twenty milligrams of CoPc/CN were placed into an EPR quartz tube and then treated under dynamic vacuum (4.5 Pa) to remove surface adsorption species. We evaluated the thickness and roughness of ultrathin porous CN nanosheets with atomic force microscopy (AFM) equipment.

### 1.3 Calculation details

The computational modeling of the CoPc/CN and Gibbs free energy of intermediates involved in the reactions were performed in the Vienna Ab Simulation Package (VASP) code.[1, 2] The core electronics were processed using the plane-wave basis set and Projector Augmented Wave method. The exchange-correlation function was exhibited by generalized gradient approximation with Perdew-Burke-Ernzerhof. Interactions between valence electrons and ionic nuclei were defined by ultrasoft pseudopotentials, the cutoff energy for the plane wave basis was set at 400 eV, and the Brillouin zone was sampled using a 2×2×1 Monkhorst–Pack grid of k-points. Considering the CoPc/CN catalytic system with ILs, we corrected the dispersion effect by DFT-D3 (BJ damping)[3]. The structural optimization was completed for energy and force convergence set at 1.0×10$^{-4}$ eV and 0.02 eV Å$^{-1}$. We set the vacuum space at 15 Å in the z direction to consider the influence of the periodic structure. The lower layer of CN is fixed to facilitate convergence. The spin polarization effect and dipole correction should be considered in the calculation process, which facilitate the transport of photogenerated electrons.

## 2. Supplementary figures and tables.

The selectivity for methanol, ethanol and hydrogen are obtained by Equations (S1)–(S3):

$$S_{CH_3OH} = \frac{n_{CH_3OH}}{n_{CH_3OH} + n_{CH_3CH_2OH} + n_{H_2}} \qquad (S1)$$

$$S_{CH_3CH_2OH} = \frac{n_{CH_3CH_2OH}}{n_{CH_3OH} + n_{CH_3CH_2OH} + n_{H_2}} \qquad (S2)$$

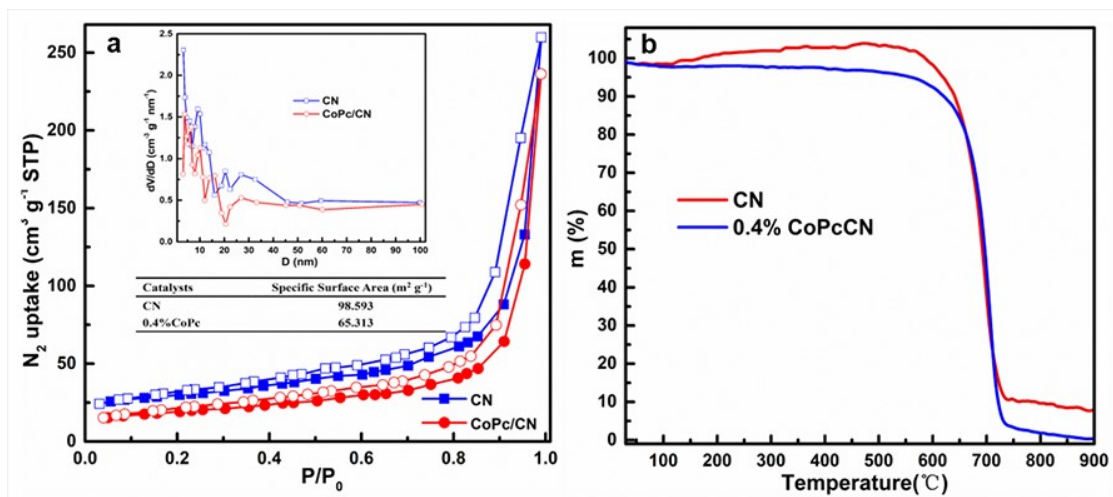$$S_{H_2} = \frac{n_{H_2}}{n_{CH_3OH} + n_{CH_3CH_2OH} + n_{H_2}} \qquad (S3)$$

Fig.S1. (a) TGA of CN and CoPc/CN, (b) $N_2$ adsorption-desorption isotherm of CN and CoPc/CN at 77 K. Solid and open circles denote adsorption and desorption respectively.
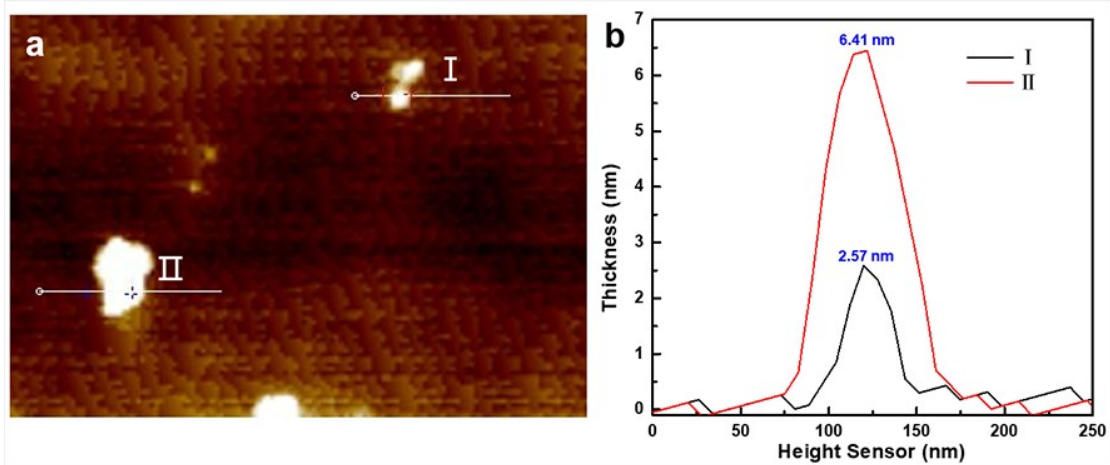
Fig.S2. (a) the AFM 2D images; (b) the corresponding height profiles of CoPc/CN.

Table S1. Co$^{2+}$ content in the CoPc/CN and CoPc/AO complexes.

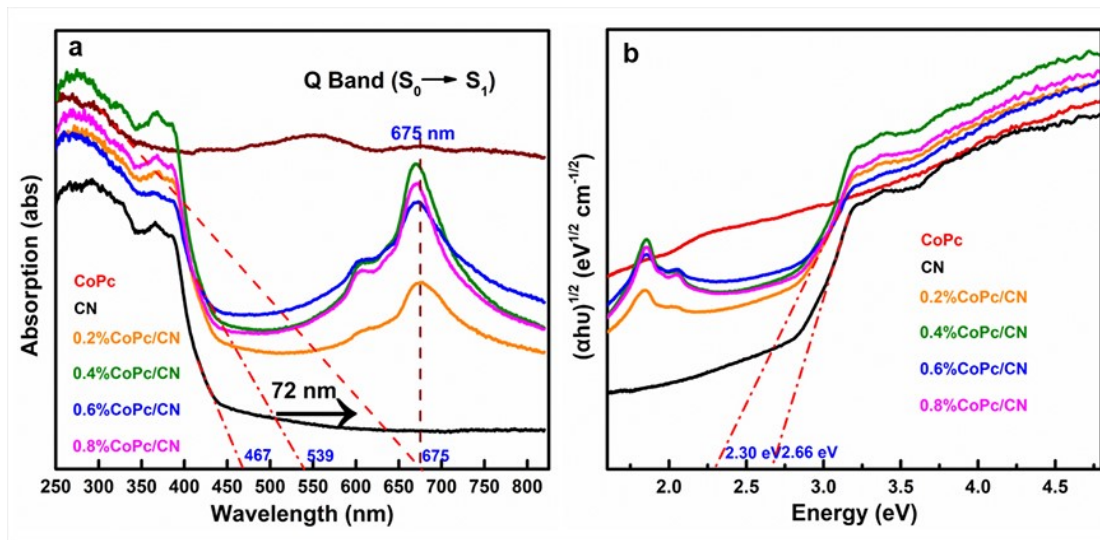| Entry | Sample | Content (%) |
|:---:|:---:|:---:|
| 1 | 0.2%CoPc/CN | 0.11397 |
| 2 | 0.4%CoPc/CN | 0.22722 |
| 3 | 0.6%CoPc/CN | 0.30674 |
| 4 | 0.8%CoPc/CN | 0.47712 |
| 5 | 0.4%CoPc/AO | 0.22302 |
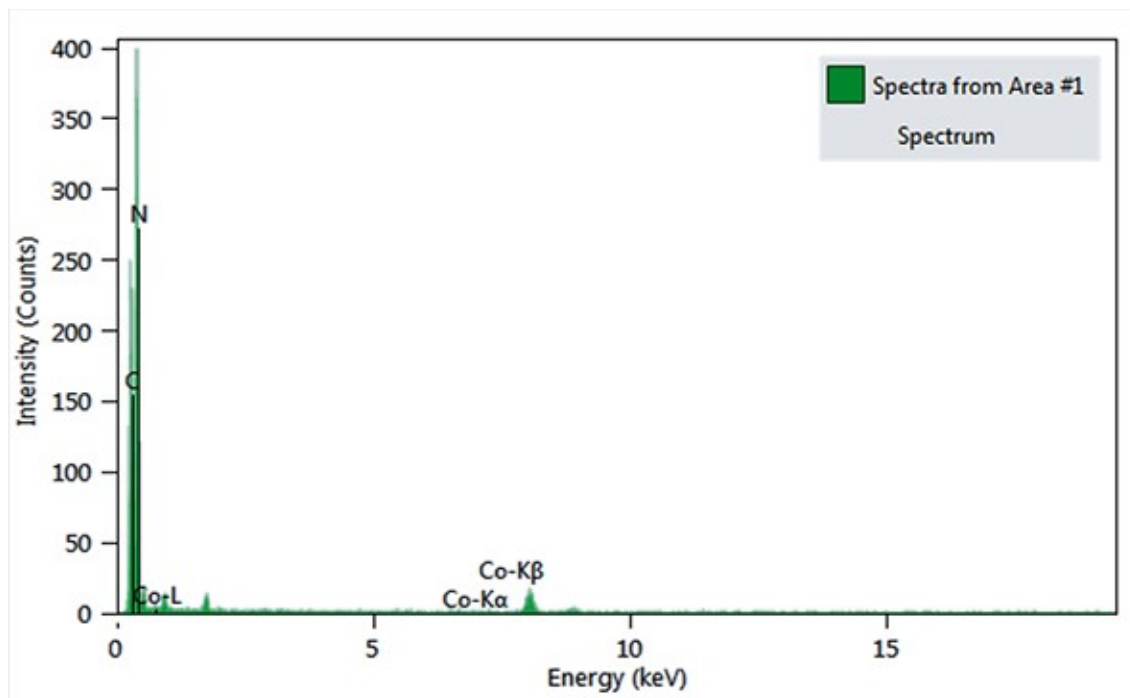
Fig.S3. EDX spectrogram of CoPc/g-C$_3$N$_4$ catalyst.

Fig.S4. (a) UV–Vis DRS spectrum of the CN-based nanocomposites; (b) the corresponding Tauc Plots
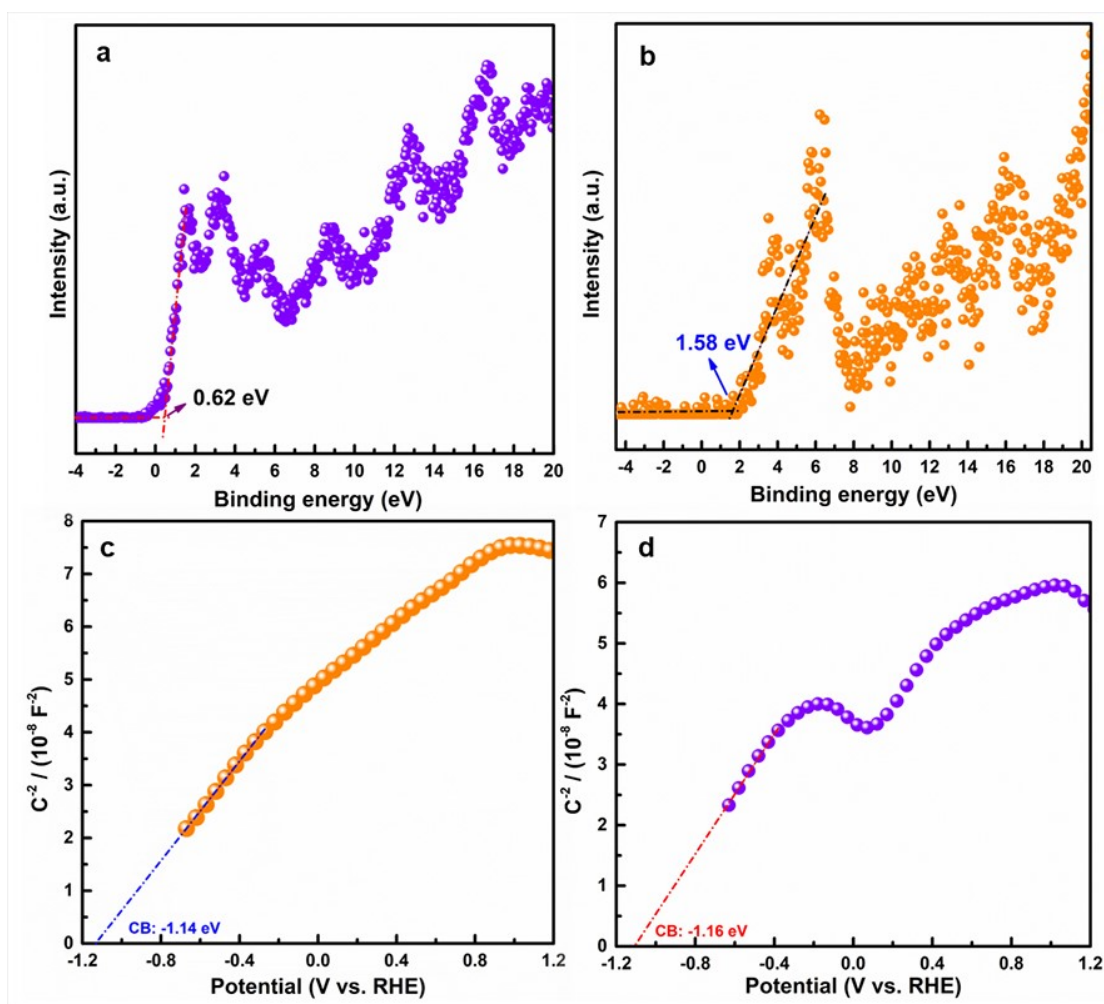
Fig.S5. the XPS-VB spectra of (a) CN and (b) CoPc, Mott-Schottky plots of (c) CN and (d) CoPc.
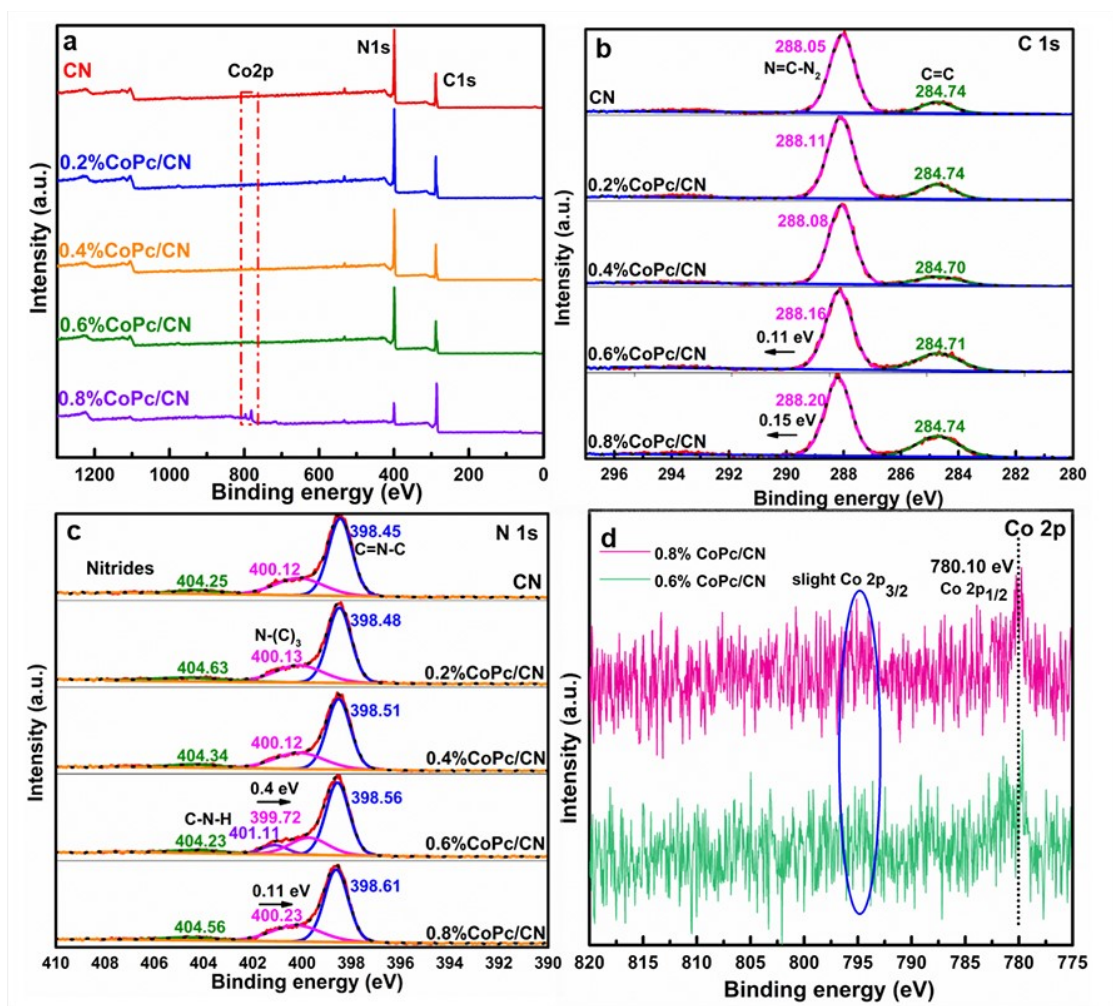
$$E_{CB} = E_{VB} - E_g \qquad (S4)$$

Fig.S6. (a) XPS survey spectra; (b) C 1s; (c) N 1s; (d) Co 2p of CN and CoPc/CN.
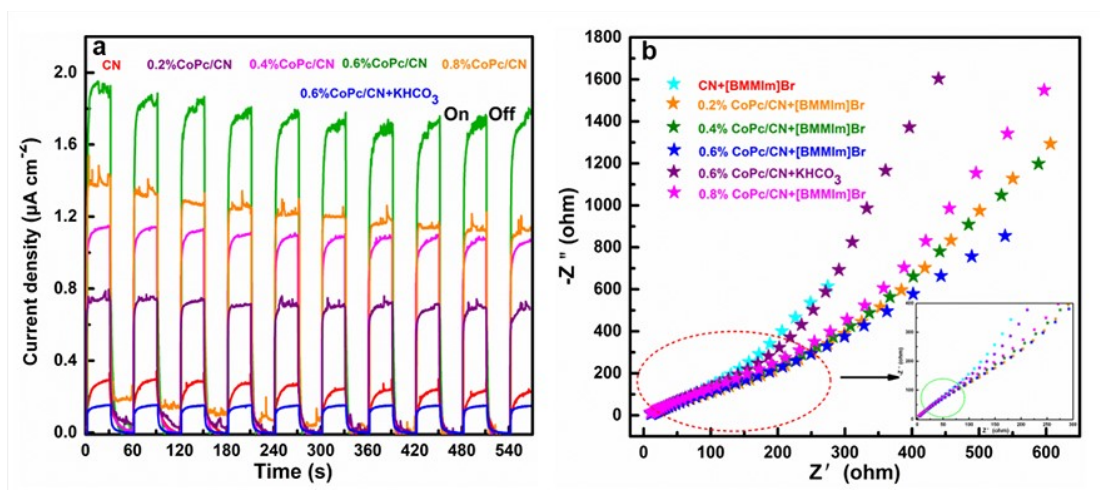
Fig.S7. (a) Photocurrent responses at open-circuit voltage, CN, 0.2%, 0.4%, 0.6%, 0.8%CoPc/CN in [BMMIm]Br electrolyte (red line, purple line, pink line, green line, orange line, respectively), 0.6%CoPc/CN in KHCO$_3$ electrolyte (b) EIS results for the CN nanosheets, 0.2%, 0.4%, sample in 0.6%, 0.8%CoPc/CN [BMMIm]Br and 0.6%CoPc/CN in KHCO$_3$ electrolyte, the insert is partial enlarged detail.
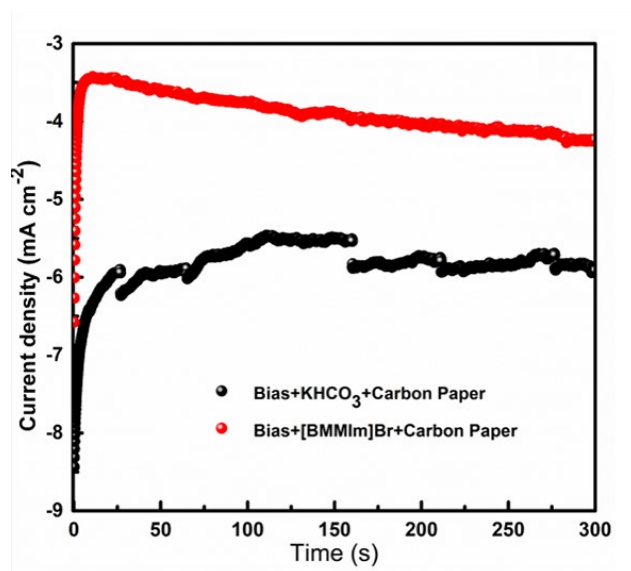
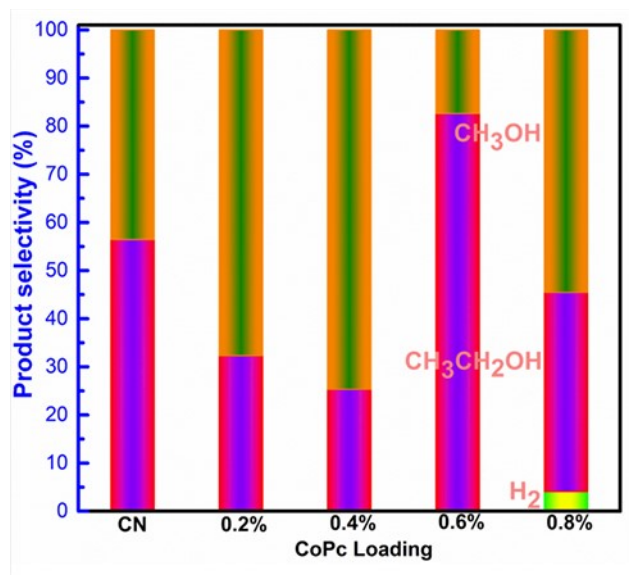Fig.S8. the current response at −1.0 V ((vs. RHE)) on 0.6%CoPc/CN in 0.1 M [BMMIm]Br and KHCO$_3$ electrolyte.

Fig.S9. Product selectivity of $CO_2$ reduction products for different CoPc loading on CN nanosheets at -1.0 V vs. RHE.

Table S2. PEC $CO_2$ reduction to alcohol over various catalysts

| Catalysts | Irradiation source | Bias [V] | Products | Rate [$\mu M\ cm^{-2}\ h^{-1}$] | Ref. |
|---|---|---|---|---|---|
| CoPc/CN | 300 W Xe lamp | -1.0 vs. RHE | Methanol/Ethanol | 6465.9/218.6 | this work |
| Pd@TiO$_2$ | 300 W Xe lamp | -0.6 vs. SCE | Methanol | 43.6 | 4 |
| Ti/TiO$_2$/phosphorene | 300 W Xe lamp | -0.8 vs. Ag/AgCl | Methanol | 250 | 5 |
| FeS$_2$/TiO$_2$ | 500 W Xe lamp | -1.2 vs. SCE | Methanol | 91.7 | 6 |
| NH$_2$-TiO$_2$/Ni | 300 W Xe lamp | -1.0 vs. SCE | Methanol | 153 | 7 |
| CuO | visible light | -0.7 vs. Ag/AgCl | Methanol/Ethanol | 50.4/10.6 | 8 |
| CuFe$_2$O$_4$/GO | visible light | -0.4 vs. Ag/AgCl | Methanol | 7.2 | 9 |
| S-TiO$_2$@GS | 300 W Xe lamp | -0.9 vs. SCE | Methanol/Ethanol | 12/20.7 | 10 |
| Cu/Cu$_2$O-Cu (BDC-NH$_2$) | 300 W Xe lamp | +0.1 vs. Ag/AgCl | Methanol | 224 | 11 |
| Au/α-Fe2O3/RGO | visible light | -0.6 vs. RHE | Methanol | 21 | 12 |
| ZnPc/CN | visible light | -1.0 vs. SCE | Methanol | 40.6 | 13 |
| Metalloporphyrin/TiO$_2$ | simulated sunlight | -0.6 vs. SCE | Methanol | 55.5 | 14 |
| M-TiO$_2$@ZnO | 300 W Xe lamp | -1.0 vs. NHE | Methanol/Ethanol | 30.5/24 | 15 |
| CeO$_2$/CuO | 500 W Xe lamp | -1.0 vs. SCE | Methanol | 3.4 | 16 |
| Bi$_2$WO$_6$/BiOCl | 300 W Xe lamp | -1.0 vs. SCE | Ethanol | 11.4 | 17 |
| Ti$_3$C$_2$/g-C$_3$N$_4$ | 300 W Xe lamp | -0.85 vs. Ag/AgCl | Formate/Methanol | 37/13.2 | 18 |
| Cu@porphyrin-COFs | 300 W Xe lamp | -1.0 vs. SCE | Ethanol | ca.16 | 19 |
| Pd@TiO$_2$/Ti$_3$CN | 300 W Xe lamp | -0.7 vs. SCE | Methanol/Ethanol | ca.7.5/7 | 20 |
| TiO$_2$/CuO | 125 W Hg lamp | +0.2 vs. Ag/AgCl | Methanol | 500 | 21 |
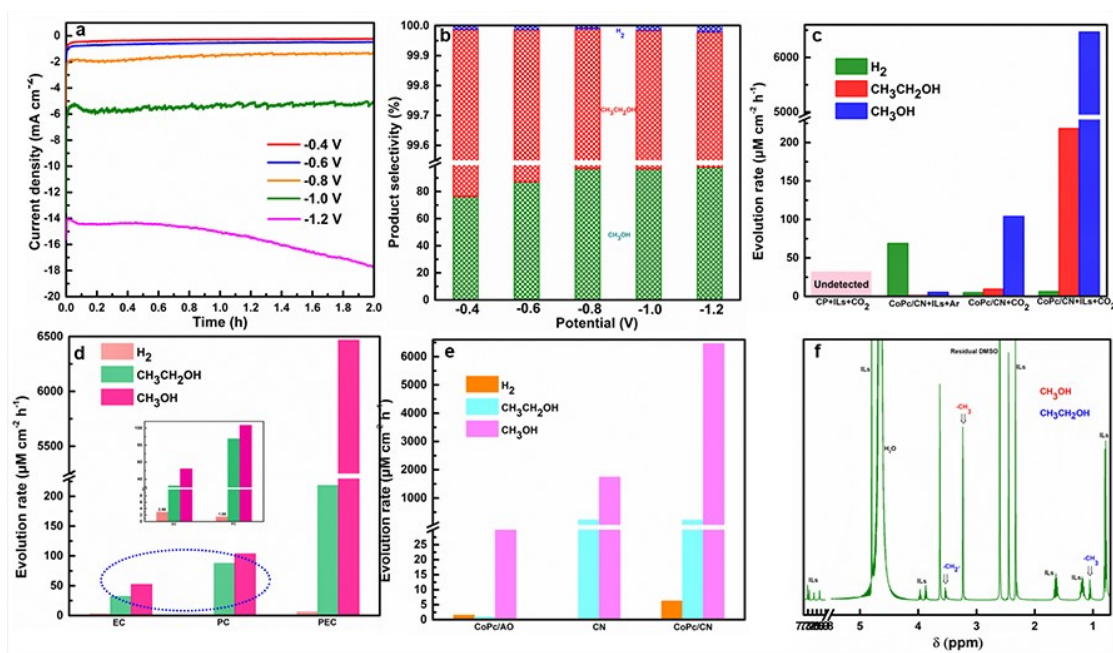
Fig.S10. (a) the representative chronoamperograms, (b) the product selectivity of $CO_2$ reduction products for 0.4%CoPc/CN at various potentials (−0.4 V−(−1.2 V) vs. RHE), (c) PEC $CO_2$ reduction to generate methanol and ethanol under different condition, (d) the rate of methanol and ethanol for photocatalytic, electrocatalytic, PEC $CO_2$ reduction. EC: 25 mg 0.4%CoPc/CN, −1.0 V vs. RHE, PC: 25 mg 0.4%CoPc/CN, 300 W Xe lamp, 25 ℃ (circulating water), PEC: 25 mg 0.4%CoPc/CN, 300 W Xe lamp, 25 ℃ (circulating water), −1.0 V vs. RHE., the insert: partial enlarged view, (e) a control performance experiment on CoPc or CN alone for PEC $CO_2$ reduction, (f) ^{1}HNMR spectrum under optimized catalytic conditions on CoPc/CN in [BMMIM]Br solution.
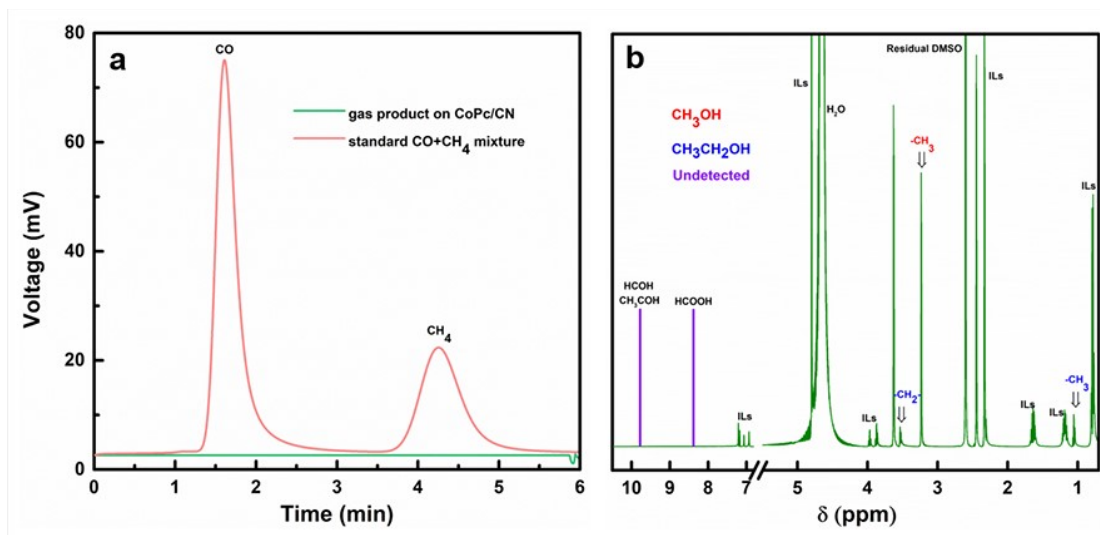
Fig.S11. (a) Chromatogram for determination of CO and CH$_4$, (b) 1H-NMR spectrum for determination of formate, formaldehyde and acetaldehyde.
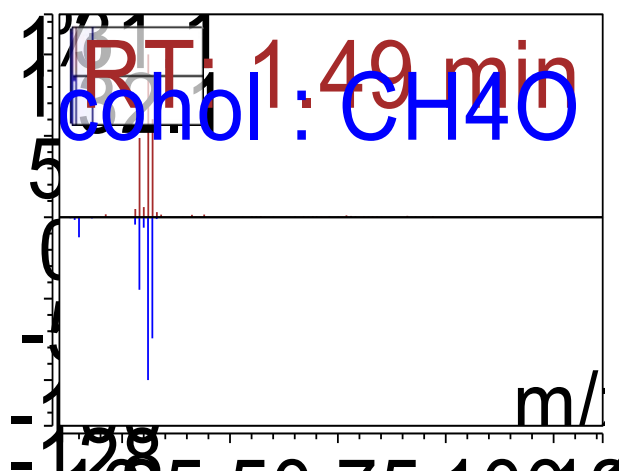
RT: 1.49 min

cohol : CH4O

m/

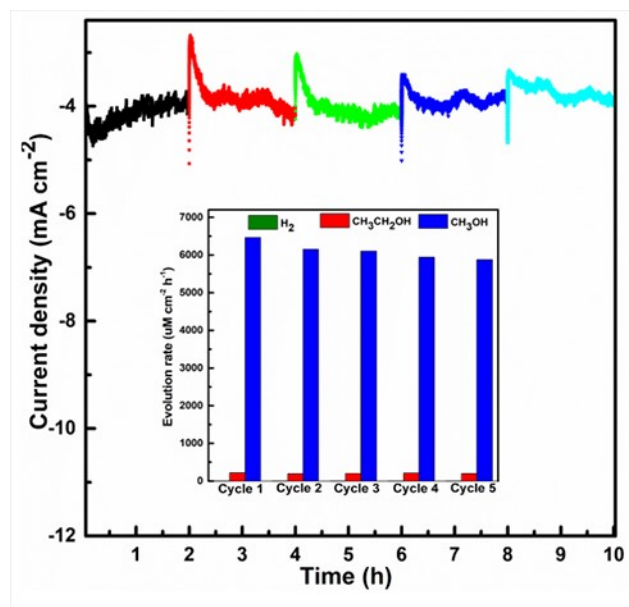Fig.S12. GC-MC spectra of methanol product under $^{12}CO_2$ atmosphere

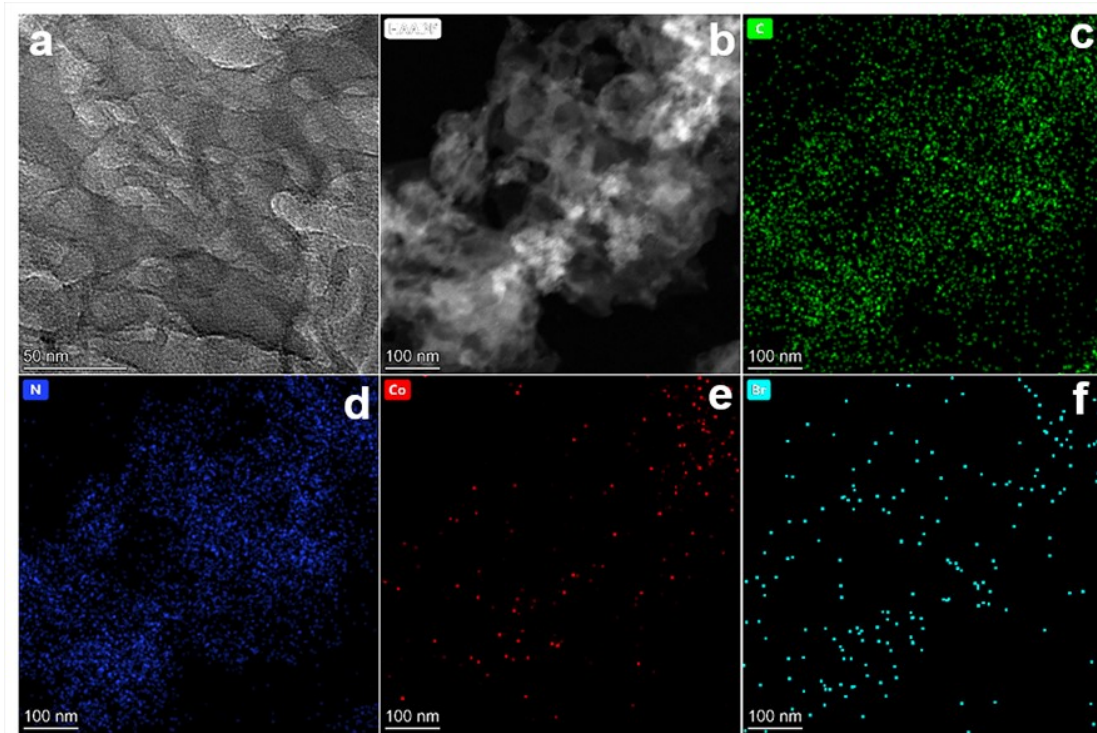Fig.S13. Cyclic experiment of CoPc/CN for PEC $CO_2$ reduction

Fig.S14. TEM and mapping images of un-fresh CoPc/CN.

# References

1. H. X. Zhong, M. Ghorbani-Asl, K. H. Ly, J. C. Zhang, J. Ge, M. C. Wang, Z. Q. Liao, D. Makarov, E. Zschech, E. Brunner, I. M. Weidinger, J. Zhang, A. V. Krasheninnikov, S. Kaskel, R. H. Dong and X. L. Feng, *Nat. Commun.*, 2020, **11**, 1409.
2. S. Sato, K. Saita, K. Sekizawa, S. Maeda and T. Morikawa, *ACS Catal.*, 2018, **8**, 4452–4458.
3. Wen Hao Ren, X. Tan, X. J. Chen, G. B. Zhang, K. N. Zhao, W. F. Yang, C. Jia, Y. Zhao, S. C. Smith and C. Zhao, *ACS Catal.*, 2020, **10**, 13171–13178.
4. Y. J. Xu, Y. J. Jia, Y. Q. Zhang, R. Nie, Z. P. Zhu, J. G. Wang and H. W. Jing, *Appl. Catal. B: Environ.*, 2017, **205**, 254–261.
5. F. A. Sayao, X. Ma, M. V. B. Zanoni and A. Lachgar, *J. Mater. Chem. C*, 2022, **10**, 11276–11285.
6. E. Han, F. Y. Hu, S. Zhang, B. Luan, P. Q. Li, H. Q. Sun and S. B. Wang, *Energy Fuels*, 2018, **32**, 4357–4363.
7. L. W. Wang, Y. J. Jia, R. Nie, Y. Q. Zhang, F. J. Chen, Z. P. Zhu, J. G. Wang and H. W. Jing, *J. Catal.*, 2017, **349**, 1–7.
8. S.-S. Liu, Q.-J. Xing, Y. Chen, M. Zhu, X.-H. Jiang, S.-H. Wu, W. Dai and J.-P. Zou, *ACS Sustainable Chem. Eng.*, 2018, **7**, 1250–1259.
9. K. M. Rezaul Karim, M. Tarek, H. R. Ong, H. Abdullah, A. Yousuf, C. K. Cheng and M. M. R. Khan, *Ind. Eng. Chem. Res.*, 2018, **58**, 563–572.
10. L. W. Wang, Y. Wei, R. Fang, J. Y. Wang, X. G. Yu, J. Z. Chen and H. W. Jing, *J. Photoch. Photobio. A: Chem.*, 2020, **391**, 112368.
11. B. C. e. Silva, K. Irikura, R. C. G. Frem and M. V. B. Zanoni, *J. Electroanal. Chem.*, 2021, **880**, 114856.
12. B. G, K. Rambabu, A. Hai, N. Ponpandian, J. E. Schmidt, D. D. Dionysiou, M. Abu Haija and F. Banat, *Appl. Catal. B: Environ.*, 2021, **298**, 120520.
13. J. G. Zheng, X. J. Li, Y. Qin, S. Q. Zhang, M. S. Sun, X. G. Duan, H. Q. Sun, P. Q. Li and S. B. Wang, *J. Catal.*, 2019, **371**, 214–223.
14. Y. P. Dong, R. Nie, J. X. Wang, X. G. Yu, P. C. Tu, J. Z. Chen and H. W. Jing, *Chinese J. Catal.*, 2019, **40**, 1222–1230.
15. B. Han, J. X. Wang, C. X. Yan, Y. P. Dong, Y. J. Xu, R. Nie and H. W. Jing, *Electrochim. Acta*, 2018, **285**, 23–29.
16. Z. B. Pan, E. Han, J. G. Zheng, J. Lu, X. L. Wang, Y. B. Yin, G. I. N. Waterhouse, X. G. Wang and P. Q. Li, *Nanomicro Lett.*, 2020, **12**, 18.
17. J. X. Wang, Y. Wei, B. J. Yang, B. Wang, J. Z. Chen and H. W. Jing, *J. Catal.*, 2019, **377**, 209–217.
18. Y. J. Xu, S. Wang, J. Yang, B. Han, R. Nie, J. X. Wang, Y. P. Dong, X. G. Yu, J. G. Wang and H. W. Jing, *J. Mater. Chem. A*, 2018, **6**, 15213–15220.
19. B. Wang, F. L. Yang, Y. P. Dong, Y. Z. Cao, J. Y. Wang, B. J. Yang, Y. Wei, W. R. Wan, J. Z. Chen and H. W. Jing, *Chem. Eng. J.*, 2020, **396**, 125255.
20. Y. J. Xu, F. Wang, S. L. Lei, Y. Wei, D. Zhao, Y. H. Gao, X. Ma, S. J. Li, S. Q. Chang, M. Q. Wang and H. W. Jing, *Chem. Eng. J.*, 2023, **452**, 139392.
21. J. F. d. Brito, F. F. Hudari and M. V. B. Zanoni, *J. $CO_2$ Util.*, 2018, **24**, 81–88.